Accepted Manuscript

Synthesis, pH dependent photometric and electrochemical investigation, redox mechanism and biological applications of novel Schiff base and its metallic derivatives

Abdul Rauf, Afzal Shah, Abdul Aziz Khan, Aamir Hassan Shah, Rashda Abbasi, Irfan Zia Qureshi, Saqib Ali

PII:	S1386-1425(17)30019-7
DOI:	doi: 10.1016/j.saa.2017.01.018
Reference:	SAA 14871
To appear in:	*Spectrochimica Acta Part A: Molecular and Biomolecular Spectroscopy*
Received date:	3 October 2016
Revised date:	7 January 2017
Accepted date:	7 January 2017

Please cite this article as: Abdul Rauf, Afzal Shah, Abdul Aziz Khan, Aamir Hassan Shah, Rashda Abbasi, Irfan Zia Qureshi, Saqib Ali , Synthesis, pH dependent photometric and electrochemical investigation, redox mechanism and biological applications of novel Schiff base and its metallic derivatives. The address for the corresponding author was captured as affiliation for all authors. Please check if appropriate. Saa(2017), doi: 10.1016/j.saa.2017.01.018

Synthesis, pH dependent photometric and electrochemical investigation, redox mechanism and biological applications of novel Schiff base and its metallic derivatives

Abdul Rauf [a], Afzal Shah [a*], Abdul Aziz Khan [a], Aamir Hassan Shah[a,b]*, Rashda Abbasi [c], Irfan Zia Qureshi[d] and Saqib Ali[a]

[a] Department of Chemistry Quaid-i-Azam University, 45320, Islamabad, Pakistan

[b]University of Chinese Academy of Sciences, Beijing 100049, China.

[c]Institute of Biomedical and Genetic Engineering Islamabad, Pakistan

[d]Department of Animal Sciences, Quaid-i-Azam University, 45320 Islamabad, Pakistan

*To whom correspondence should be addressed

Tel: +92-5190642110

Fax: +92-5190642241

E-mails: afzals_qau@yahoo.com (Dr. Afzal Shah) aamir@nanoctr.cn (Dr. Aamir Hassan Shah)

Abstract

A novel Schiff base, 1-((2, 4-dimethylphenylimino)methyl)naphthalen-2-ol abbreviated as (HL) and its four metallic complexes were synthesized and confirmed by ^{1}H and ^{13}C NMR, FTIR, TGA and UV–Visible spectroscopy. Schiff base was also characterized by X-ray analysis. The photometric and electrochemical responses of all the synthesized compounds were investigated in a wide pH range. Structures of the compounds were optimized computationally for the evaluation of different physico-chemical parameters. On the basis of electrochemical results the redox mechanistic pathways of the compounds were proposed. The cytotoxicity analysis on Hela cells revealed that HL and its complexes inhibit cell growth as revealed from their IC50 values (HL):106.7 µM, (L_2VO): 40.66 µM, (L_2Sn): 5.92 µM, (L_2Zn): 42.82 and (L_2Co): 107.68 µM. The compounds were tested for anti-diabetic, triglyceride, cholesterol, anti-microbial, anti-fungal and enzyme inhibition activities. The results revealed that HL and its complexes are promising new therapeutic options as these compounds exhibit strong activity against cancer cells, diabetics, fungal and microbial inhibition.

Keywords: Schiff base; Metal-Schiff base complexes; Redox mechanism; Charge transfer; Biological activities

1. Introduction

Schiff bases are nitrogenous class of organic compounds, also known as imines or azomethines. Their antibacterial, anticancer, antitumor, anti-inflammatory, anti-tuberculosis, insecticidal, antimicrobial and anticonvulsant activities are extensively reported [1-3] as they find applications against a number of organisms including *plasmopora viticola, candida albicans, bacillus polymxa, mycobacteria, trychophyton gypseum, erysiphe graminis* and *escherichia coli staphylococcus aureus*. Aromatic Schiff bases have a wide variety of applications in medicinal and inorganic chemistry [4]. They are used for enhancing the sensitivity and selectivity of electrochemical and optical sensors due to their redox and optical properties [5-7]. Their metal complexes serve as models for anticancer and herbicidal applications [8, 9]. *O-phenylenediamine* based Schiff bases are bestowed with clinical properties. Schiff base obtained from p-toluidene and furylglyoxal has been reported for its excellent inhibitory action against *bacillus subtilis, escherichia coli, staphylococcus aureus and proteus vulgaris* [10]. Schiff bases of 4-dimethylamine benzaldehyde are potent antibacterial agents. Isatin Schiff bases possess antiviral, antiprotozoal, anti-HIV, anticonvulsant and anthelmintic activities. Some Schiff bases are also used as antibodies and anti-inflammatory agents [11-14]. Based on the above mentioned broad range applications, pharmacologists and biochemists are paying the utmost attention to the synthesis of new medicinally important Schiff bases [15, 16].

Schiff bases can act as good chelating agents, [17, 18] especially when –OH or –SH functional groups are present in their structures. A plethora of biological, industrial, analytical and environmental applications of metal complexes of Schiff base ligands have been reported [16], so, synthesis of new candidates of this class and detailed investigations of their optical and redox activities related to their biological role seems conceivable. With this aim we synthesized a

novel Schiff base, 1-((2, 4-dimethylphenylimino)methyl)naphthalen-2-ol and its complexes with VO, Sn, Zn and Co. In electrochemical sensors, Schiff bases are used as components of the recognition layer for the selective and sensitive detection of metal ions [19, 20]. So, we investigated the redox behavior of our synthesized Schiff base and its metal complexes for getting insights about their medicinal, biological and metal ions sensing role. Computational studies were also performed and interestingly the theoretical calculations were found to support the experimental outcomes.

2. Experimental

2.1. Chemicals

Acetic acid, ethylenediaminetetraacetic acid disodium salt dihydrate (Na_2 EDTA), 2-hydroxy-1-naphthaldehyde, 2,4-dimethylaniline, dibutyltindichloride, L-glutamine, penicillin-G, pyruvic acid, sodium chloride, sodium dodecyl sulfate (SDS), streptomycin sulfate, sulforhodamine B (SRB), trichloroacetic Acid (TCA), trypsin/EDTA (5%), vanadyl(V) isopropoxide, zinc acetate, cobalt acetate and magnesium chloride were received from Aldrich, USA. The solvents like toluene, chloroform, n-hexane, ethanol and dimethyl sulfoxide were obtained from Merck, Germany and dried before use. Diethanolamine and *p*-nitrophenyl phosphate hexahydrate were used as received from Sigma Aldrich. Human serum was used as a source of alkaline phosphatase.

2.2. Synthesis

2.2.1 1-((2, 4-dimethylphenylimino)methyl)naphthalen-2-ol (HL)

Stoichiometric amounts of 2,4-dimethylbenzenamine and 2-hydroxy-1-naphthaldehyde (5 mmol of each) were added to freshly dried ethanol. The mixture was refluxed for 2 hrs. The obtained

yellow crystalline solid was cooled, filtered and crystallized in a mixture of chloroform and pet ether (3:1) (**Scheme 1**). The formation of HL was ensured from the following data.

Yield: 85 %, **M.P.:** 155.5 ^{o}C; **Mol. Wt.:** 275.33, **IR υ/cm^{-1}:** 3446 (OH), 1615 (C=N), 1299 (C-O). **^{1}H NMR ($CDCl_3$, 300 MHz) δ**: 15.09 (s, 1H, -OH), 9.27 (s, 1H, H9, HC=N), 7.24 (d, 1H, H3, *J* = 1.2 Hz) 7.09-7.12 (m, 3H, H5, H6, H12), 2.35 (s, 3H, H7), 2.44 (s, 3H, H8), 8.07 (d, 1H, H13 *J* = 8.8 Hz), 7.67 (d, 1H, H15, *J* = 8.8 Hz), 7.30 (d, 1H, H16, *J* = 8.0 Hz), 7.50 (d, 1H, H17, *J* = 8.0 Hz), 7.69 (d, 1H, H18, *J* = 8.0 Hz); **^{13}C NMR (75 MHz) δ**: 140.6 (1C, C1), 130.7 (1C, C2), 133.3 (1C, C3), 136.8 (1C, C4), 127.8 (1C, C5), 118.6 (1C, C6), 18.1 (1C, C7), 21.0 (1C, C8), 171.7 (1C, C9), 108.6 (1C, C10), 153.1 (1C, C11), 116.9 (1C, C12), 131.8 (1C, C13), 129.3 (1C, C14), 128.0 (1C, C15), 122.7 (1C, C16), 127.0 (1C, C17), 123.4 (1C, C18), 136.4 (1C, C19).

By using HL as a ligand, its four metal complexes were also synthesized according to **Scheme 2**.

2.2.2 Oxovanadium(IV) complex of 1-((2,4-dimethylphenylimino) methyl)naphthalen-2-ol (L_2VO)

Oxovanadium complex (L_2VO) was synthesized by treating the vanadyl(V) isopropoxide with HL in 1:2 using acetonitrile as a solvent at room temperature as shown in **Scheme 2**. The green colored product (L_2VO) was precipitated out immediately, filtered, washed with acetonitrile and then air dried.

Complex (L_2VO) : Yield: 76 %, **M.P.:**> 300 ^{o}C; **Mol. Wt.**: 615.61, **IR υ/cm^{-1}:** 1599 (C=N), 1301 (C-O), 978 (V=O), 572 (V-O). **μ_{eff}** (BM) 2.04. **Anal. Calc. for** [$C_{38}H_{32}N_2O_3V$] (%); C, 74.14; H, 5.24; N, 4.55; O, 7.80; **Found:** C, 74.55; H, 5.20; N, 4.52; O, 8.01

2.2.3 Dibutyltin complex of 1-((2,4-dimethylphenylimino)methyl) naphthalen-2-ol (L_2Sn)

Dibutyltin complex (L_2Sn) was synthesized by refluxing the dibutyltindichloride with HL in 1:2 ratio using toluene as a solvent at elevated temperature for four hours. The yellow solution was concentrated by the process of evaporation under reduced pressure to get the precipitates of (L_2Sn).

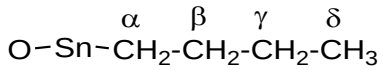

Complex (L_2Sn) : Yield: 70 %, **M.P.:** 249.3^{o}C; **Mol. Wt.**: 781.61 , **IR υ/cm^{-1}:** 1590 (C=N), 1303 (C-O), 540 (Sn-C), 551 (Sn-O), 452 (Sn-N). **^{1}H NMR ($CDCl_3$, 300 MHz) δ:** 9.28 (s, 1H, H9, HC=N), 7.28 (s, 1H, H3), 7.11-7.15 (m, 3H, H5, H6, H12), 2.39 (s, 3H, H7), 2.49 (s, 3H, H8), 8.10 (d, 1H, H13, *J* = 8.4 Hz), 7.72 (d, 1H, H15, *J* = 7.8 Hz), 7.35 (t, 1H, H16, *J* = 8.1 Hz), 7.54 (t, 1H, H17, *J* = 8.1 Hz), 7.82(d, 1H, H18, *J* = 8.4 Hz); 1.40-1.48 (m, 2H, αH) 1.78-1.85 (m, 4H, βH, γH), 0.97 (t, 3H, δH, *J* = 7.2 Hz). **^{13}C NMR (75 MHz) δ:** 140.2 (1C, C1), 130.7 (1C, C2), 133.4 (1C, C3), 137.2 (1C, C4), 127.8 (1C, C5), 118.6 (1C, C6), 18.1 (3C, C7), 21.0 (3C, C8), 172.6 (1C, C9), 117.0 (1C, C10), 154.0 (1C, C11), 118.6 (1C, C12), 131.9 (1C, C13), 129.4 (1C, C14), 128.2 (1C, C15), 123.1 (1C, C16), 127.0 (1C, C17), 123.5 (1C, C18), 136.6 (1C, C19), 26.8 (2C, αC), 26.9 (2C, βC), 26.3 (2C, γC), 13.5 (3C, δC), ^{1}J = 423.75/405.0 Hz ($^{119/117}$Sn, ^{13}C).

2.2.4 Zinc complex of 1-((2,4-dimethylphenylimino)methyl) naphthalen-2-ol (L_2Zn)

Zinc complex (L_2Zn) was synthesized by adding zinc acetate in HL solution in 1:2 using ethanol as a solvent at room temperature. The yellow colored product (L_2Zn) was precipitated out in 5-10 minutes, filtered, washed with ethanol and then air dried.

Complex (L2Zn) : Yield: 78 %, **M.P.:**173 ^{o}C; Mol. Wt.:614.06 , **IR υ/cm^{-1}:** 1591 (C=N), 1310 (C-O), 474 (Zn-O), 465 (Zn-N). **^{1}H NMR ($CDCl_3$, 300 MHz) δ:** 9.30 (s, 1H, H9, HC=N), 7.30 (s, 1H, H3), 7.13-7.16 (m, 3H, H5, H6, H12), 2.35 (s, 3H, H7), 2.44 (s, 3H, H8), 8.09 (d, 1H, H13, *J* = 8.4 Hz), 7.70 (d, 1H, H15, *J* = 7.8 Hz), 7.33 (t, 1H, H16, *J* = 8.1 Hz), 7.56 (t, 1H, H17, *J* = 8.1 Hz), 7.80(d, 1H, H18, *J* = 8.4 Hz). **^{13}C NMR (75 MHz) δ:** 140.1 (1C, C1), 130.6 (1C, C2), 133.3 (1C, C3), 136.9 (1C, C4), 127.8 (1C, C5), 118.6 (1C, C6), 18.1 (3C, C7), 21.0 (3C, C8), 171.8 (1C, C9), 108.5 (1C, C10), 155.1 (1C, C11), 117.0 (1C, C12), 129.5 (1C, C13), 129.3 (1C, C14), 128.1 (1C, C15), 122.8 (1C, C16), 127.0 (1C, C17), 123.4 (1C, C18), 136.4 (1C, C19).

2.2.5 Cobalt complex of 1-((2,4-dimethylphenylimino)methyl) naphthalen-2-ol (L_2Co)

Cobalt complex (L_2Co) was synthesized by treating cobalt acetate with HL in 1:2 ratio using ethanol as a solvent at room temperature according to **Scheme 2.** The reddish brown colored product (L_2Co) was precipitated out in few minutes, filtered, washed with ethanol and then air dried. The formation of oxovanadium and cobalt complex was ensured from the following thermo gravimetric analysis (TGA) data shown in **Table 1**.

Complex (L2Co) : Yield: 80 %, **M.P.:**183 ^{o}C; **Mol. Wt.:** 607.61 , **IR υ/cm^{-1}:** 1600 (C=N), 1305 (C-O), 474 (Co-O), 507 (Co-N). **μ_{eff}** (BM) 1.81. **Anal. Calc. for** [$C_{38}H_{32}N_2O_2Co$] (%); C, 75.12; H, 5.31; N, 4.61; O, 5.27; **Found:** C, 75.35; H, 5.22; N, 4.75; O, 5.43.

(TGA data is given in Table 1)

2.3. X-ray structure determination and UV-Vis spectroscopic measurements

Suitable single crystal HL was mounted on a Microstar diffractometer. Data were collected by keeping the temperature constant at 100 K. The structural calculations were solved with the

olex2 using Charge Flipping program and refined with XL [21] refinement packages using the least squares minimization. Crystal data and details of the parameters are summarized in **Tables S1-S3**. Shimadzu 1601 spectrophotometer was used for UV-visible spectroscopic studies. Crison micro pH 2001 pH-meter was used for pH measurements. Before each experiment fresh solution was prepared from stock solution using 50% ethanol and 50% BR buffers.

2.4. Anti-diabetic Activity

Fifty BALB/c healthy adult male mice with an average body weight of 35.0±5.0 g were procured from the National Institute of Health Islamabad. To reduce stress and avoid overcrowding, five animals were housed per cage. All animals had free access to standard diet of rodents and drinking water. Standard temperature of 28 °C and 12hL: 12hD photoperiod was maintained throughout. Animals were subjected to diabetic disease through alloxan monohydrate (Sigma Aldrich, USA) using a single intraperitoneal injection (i.p.) at the dose of 150 mg/kg b.w. Diabetic level was achieved at glucose concentration > 200 mg/dl. A total of seven experimental groups were constituted and each containing five animals. All groups were made diabetes's above. Five groups were treated with five different compounds; HL, 1, 2, 3, and 4 at the dose of 35.0 mg/kg b.w. The remaining two groups; positive control group and negative control group were treated with glibenclamide (10mg/kg b.w in distilled H_2O), (Euglucon, Roche Pharma) and normal saline respectively. Blood was extracted through caudal vein at nine different times i.e. -1 (prealloxan), 0 (post alloxan) and 1-7 hrs after treatment with doses. Plasma glucose level was measured with dextrostix strips using glucometer (Accu-Check Active,Roche). Serum triglycerides and cholesterol were measured through commercially kits which were obtained from Globe Diagnostic (Italy), using the standard procedure of colorimetry. One-way analysis of variance (ANOVA) was used for data analysis using Sigma Plot (Version 12.0), Post hoc Tukey-

kramer test, and where test for normality failed ANOVA on ranks test was applied. Statistically significant difference was considered where $P<0.05$. Data are presented as line or bar graphs.

2.5. Cytotoxicity

2.5.1. *In-Vitro* studies: Cell line and cell culture

Human cervix adenocarcinoma (HeLa, ATCC CCl-2) cell line was cultured in Dulbecco's Modified Eagle Medium (DMEM) supplemented with GPPS (2 mM L-glutamine, 1 mM Na-pyruvate, 100 U/ml penicillin and 100 µg/ml streptomycin) and 10 % fetal calf serum under a humidified atmosphere at 5% CO_2 and 37 °C. Cells were harvested by trypsinization (0.5 mM trypsin/EDTA) for 60 sec at 25°C.

2.5.2. Cytotoxicity analysis on HeLa

Cytotoxicity caused by the compounds was tested on HeLa cells by the SRB assay as described earlier [22]. Briefly, pre-seeded cultures (>90% viability; 1.5×10^5 cells/ml) were exposed to the different compound concentrations (150, 100, 50, 10 and 5 µM) for 24 h. Untreated cultures, solvent (5% DMSO in ethanol) treated and non-cellular background comprising of 'media-only' and 'compounds-only' samples were also included in each of the experiment. Cultures were fixed by adding gently, 50% pre-chilled TCA and incubation at 4 °C for 1 h followed by washing with deionized water and air-drying. Plates were stained with 0.4% SRB solution, rinsed with 1% acetic acid and then air-dried. Samples were photographed with Olympus IMT-2 inverted microscope (magnification 60X) equipped with digital camera. The incorporated dye was dissolved in 10 mM Tris (pH 8.0) and absorbance was measured on AMP PLATOS R-496 microplate reader at 565 nm wavelength.

Percent viability of the treated and untreated samples was calculated relative to the untreated control sample using the following formula

Percent viability = [Abs $(565)_{\text{Test samples}}$ - Abs $(565)_{\text{Compound only}}$ / Abs $(565)_{\text{Untreated control}}$ - Abs $(565)_{\text{Media only}}$] × 100

Where Abs $(565)_{\text{Test samples}}$ and Abs $(565)_{\text{Untreated control}}$ represent the OD at 565 nm for the treated samples and untreated control samples, respectively. Abs $(565)_{\text{Compound only}}$ and Abs $(565)_{\text{Media only}}$ represent background OD and was measured in non-cellular background samples.

2.6. Assay of alkaline phosphatase activity

HL and its four complexes were applied to investigate their inhibitory action against the enzyme Alkaline Phosphatase by using the reported procedure [21]. Reagent A (Diethanolamine pH 9.82 along with 0.5mmol/dm^3 magnesium chloride) and reagent B (50 mmol/dm^3 *p*-nitrophenyl phosphate) were mixed with 4:1 to make substrate. After incubation of 300 sec at 25 °C, 40 µL of human serum was added in 2 mL of the substrate. Absorbance was recorded after incubation of 60 sec to check the activity of enzyme. ALP produced yellow colored product (*p*-nitrophenol) by hydrolyzing the *p*-NPP (**Scheme 3**). Various amounts of HL (20 µL, 40 µL, 60 µL, 80 µL) were added periodically from the stock solution, incubated for 180 sec and absorbance was recorded after 1 to 5 minutes. Percentage inhibition was calculated from the average of these measurements. The same procedure was repeated for each metal complex.

2.7. Antimicrobial activities

The fungicidal and bactericidal activities of HL and its metallic complexes were carried out by disc diffusion method [23]. The nutrient agar and potato dextrose agar were used as growth culture media for antibacterial and antifungal tests, respectively. The biologically active samples

formed clear zones of inhibition around the discs. The zones were measured in millimeters using a zone reader.

2.9. Electrochemical studies

Electrochemical investigations were carried using μAutolab running with GPES 4.9 software, Eco-Chemie, the Netherlands. Glassy carbon, Ag/AgCl (3 M KCl) and platinum wire were used as working, reference and counter electrodes. The working electrode was centrally placed to keep a minimum distance between the counter and reference electrodes for minimizing the IR drop effect. The surface of working electrode was polished using diamond spray (particle size 1 μm) followed by thorough rinsing with doubly distillated water before every experimental assay [24]. All electrochemical experiments were carried out under nitrogen saturated solutions.

3. Results and Discussion

3.1. Spectroscopic characterization of the synthesized compounds

In the FTIR spectrum the strong absorption band at 1615 cm^{-1} due to azomethine group shows the formation of Schiff base (HL). Moreover, the appearance of resonance signals at 9.27 ppm and 172.1 ppm in ^{1}H and ^{13}C NMR spectra confirms the formation of HL. Absence of any resonance peak related to primary amine suggests the purity of the synthesized product. In case of metal complexes, the absorption bands corresponding to azomethine group in the FTIR spectra appearing at lower wavelengths in the range of 1591-1600 cm^{-1} suggests the coordination of azomethine nitrogen with metal atoms. Data obtained from elemental analysis and thermo gravimetric analysis of L_2VO and L_2Co were found in good agreement and indicate the

formation of these complexes. For tin and zinc complexes, downfield shifting of azomethine group (HC=N) resonance signals was observed and disappearance of proton resonance signal of hydroxyl group confirmed the bonding of ligand anion with the metallic cationic parts. Moreover, Sn-C coupling constant for dibutyltin complex was calculated from the satellite peaks that appeared at 23.9 and 29.6 ppm in ^{13}C NMR spectrum.

The molecular structure of HL along with crystallographic numbering scheme is shown in **Fig. S1**. Summary of crystal data and details of structural refinements can be seen in **Table S1**. Selected bond distances and bond angles of HL are listed in **Table 2**. It is evident from the data that Schiff base has monoclinic structure. Double bond between C and N can be ensured from the shorter N-C11 bond length as compared to N-C12 bond length. Position of H1 represents that HL exists in zwitterionic form as well as in enolic form (Fig. S1). Intramolecular hydrogen bonding is present between H atom of hydroxyl group and N atom in enolic as well zwitterionic forms (**Table 3**). Tortional angles reveal that the molecular geometry is non-planar. The aromatic rings are not in the form of regular hexagons due the attached moieties.

UV-visible spectra of HL, L_2VO, L_2Sn, L_2Zn and L_2Co in a 9:1 mixture of ethanol and DMSO are displayed in **Fig. 1**. HL shows four bands at 318, 350, 442 and 461 nm. The first band around 318 nm can be related to π-π* transition of the aromatic chromophore containing azomethine group. While the second less intense band at 350 nm may be attributed to n- π* transition of the non-bonding electrons present on the nitrogen of –C=N group [25]. The signals at 442 and 461 nm are possible to emerge as a result of π-π* and n- π* transitions of the aromatic chromophore containing -C=O group. This attribution is in line with the crystal studies which offer evidence about the presence of keto group in the structure of HL. Further observation of Fig. 1 reveals that the orbital energies of HL change upon complexation with metals. The

appearance of a band in the wavelength range of 260-270 nm in the spectra of complexes and its absence in the spectrum of HL offers a convincing proof for the formation of metal-HL complexes. This band may emerge due to possible charge transfer (CT) from a metal centered orbital to a ligand centered orbital (MLCT) or vice versa (LMCT) [25-27]. The decrease in the intensity of signals corresponding to azomethine nitrogen and carbonyl oxygen suggests the charge transfer bands of L_2VO, L_2Zn and L_2Co to be LMCT in nature. While the increase in absorbance of these chromophores in the UV-Vis spectrum of L_2Sn points to the MLCT characteristic of the charge transfer band corresponding to this complex. Such a behavior also highlights the importance of back bonding/donation [27]. The molar extinction coefficient (ε) values of L_2VO, L_2Zn, L_2Sn and L_2Co evaluated from their CT bands are 4.15×10^4, 3.90×10^3 3.50×10^3, 3.35×10^3 m^2 $mole^{-1}$ respectively. These values suggest that among the studied complexes, VO and Co are the strongest and weakest acceptors of electrons from HL. Further observation of the spectra shown in Fig. 1 reveals the appearance of broad bands around 500 nm. These less intense bands compared to CT signals are attributable to d-d transition [28]. The extinction coefficients evaluated from signals corresponding to d-d transition can help in predicting the geometry of complexes. The expected ε values of octahedral complexes remain less than 10 m^2 mol^{-1}, for square planar complexes their range is around 10-500, while for tetrahedral complexes, molar extinction coefficient exceeds 500 m^2 mol^{-1} [29]. Based on these criteria, we speculate our synthesized complexes L_2VO and L_2Co (ε values 250 and 450 m^2 mol^{-1}) to have square planar geometry. However, the geometry of L_2Zn and L_2Sn cannot be predicted as no d-d band appears in the spectra of these complexes.

Fig. S2-A represents the absorption spectra of HL in different pH media. HL has shown an intense doublet band at 321 nm. Increase in pH of the medium results in hypochromic effect and

a new band appears at 414-461 nm which further shifts to 396 nm at pH > 9. The appearance of this new band can be related to the deprotonation of HL. An isosbestic point at 371 nm also appears in the spectra which suggest the transformation of HL into different isomers. Tin complex shows similar photometric response with two isosbestic points at 298 and 374 nm, thus, offering clues about the existence of its different mesomeric forms (**Fig. S2-B**). No significant change was observed in the photometric studies of complexes (L_2VO), (L_2Zn) and (L_2Co) in different pH media.

3.2. Electrochemical studies

Cyclic voltammetric behavior of I mM solution of HL and its complexes was examined at a scan rate of 100 mV s^{-1} in media different of pH using GCE as working electrode. In solution of pH 7.0, HL registered two oxidation signals at +0.76 V and +1.01 V in the forward scan with no peak in the reverse scan, thus, ensuring irreversibility of both the oxidation processes. The oxidation signals were found independent of each other as shown in **Fig. S3**. While scanning the potential from zero to negative going direction, one reduction peak of HL at -0.94 V was observed in solution conditions of pH 7.

In order to investigate the influence of medium on the redox behavior of HL, cyclic voltammograms were recorded in different pH media. It was found that redox nature of HL is strongly pH dependent as shown in **Fig. 2**. In acidic solution (pH-4.0) there was no change in oxidation peaks while the reduction peak of HL splitted into three well defined peaks. In basic medium (pH-10.0), the two oxidation peaks overlapped and converted into a single broader peak at +0.83 V. While no significant shift in reduction peak was observed with change in pH. However in acidic medium a new reduction peak at -1.13 V came to sight. **Fig. S4** depicts the cyclic voltammograms of HL and its complexes in a buffered medium of pH 7.0. In case of all

metal complexes, the two oxidation peaks overlap and result into one broader peak at +0.76 V, +0.79 V, +0.74 V and +0.79 V for L_2VO, L_2Sn, L_2Zn and L_2Co respectively. In the negative potential window instead of one sharp cathodic signal, two overlapping peaks appeared for L_2VO, L_2Sn and L_2Co. Compound L_2Zn registered a sharp reduction peak at -0.44 V and the reduced product showed irreversible oxidation at -0.24 V (**Fig. S5**). The shifting of peaks with the change in pH of solutions offers a clear evidence of the pH dependent nature of all these redox processes (**Fig. 2 & S5**).

The effect of scan rate on the cyclic voltammetric response was monitored for all the synthesized compounds in pH-7.0. By using Randles-Sevcik equation, diffusion coefficients were calculated from the slopes of the plots between I_p and $\upsilon^{1/2}$. The straight lines of the plots suggested the diffusion controlled nature of the redox processes [30-33]. CVs of different concentrations of analytes were obtained and used for the calculation of electron transfer rate constant (k_s) using the following equation [34].

$$I_p = nFACk_s$$

Where n represents number of electrons, calculated from DPV studies and A the surface area of working electrode. k_s was calculated from the slope of I_p *versus* concentration plot (**Fig. S6**). The values of diffusion coefficients and k_s for HL, L_2VO, L_2Sn, L_2Zn and L_2Co are given in **Table 4**.

To ensure the reversible/irreversible nature of the redox processes of HL and its complexes, square wave voltammetric response was observed. The same direction of forward and backward current components of all the redox processes (**Fig. S7**) offered clues about their irreversible nature. These results are consistent with the cyclic voltammetric findings. Due to its sensitive nature, SWV was used for the estimation of the limit of detection (LOD) and the limit

of quantification (LOQ) by observing the effect of concentration on peak current values of the analytes (**Fig. 3**). The LOD and LOQ values are given in **Table 5**.

As the redox processes were found pH dependent, so their differential pulse voltammetric response was investigated in a wide pH range of 2-12. The no. of electrons was calculated from half peak width values for irreversible processes using the following equation [35].

$$W_{1/2} = \frac{3.52\ RT}{\alpha nF}$$

Fig. 4 shows the DPVs for oxidation of HL and its cobalt complex. In strong acidic media, two well defined pH dependent oxidation peaks are observed. Intensity of 1st oxidation peak started decreasing with the increase in pH and finally it disappeared pH higher than 4.0, while the 2nd oxidation peak intensified and became broader with increasing pH. In all other metal complexes, the same two oxidation signals were observed but peak 3a was not present in all cases. Vanadium complex of HL showed a new pH dependent oxidation signal at low potential value of +0.26 V in strongly acidic solutions. Shifting of peak 2a with pH is significant up to pH-5.0, after that it shows no involvement of proton during electron transfer; hence it was used to calculate the pKa values of the compounds [36]. Shifting of peak potential towards more negative potential explains the facile oxidation of the analytes with increase in pH. A new pH independent and broad oxidation peak in the range of pH 4.0-9.0 ensured another one electron oxidation step of HL without involvement of proton. Number of protons involved in each process was calculated using the following equation [35].

$$dE_p/dpH = 0.059/\alpha n$$

Slopes of Ep vs pH plots were used to calculate the number of protons involved in the oxidation processes of HL and its complexes (**Fig. 5**).

Fig. S8 and S9 show DP voltammograms of reduction processes of HL and its complexes. In the negative potential window, HL registered two pH dependent signals in the acidic pH range while no signal in basic media. Shifting of peak potential to more negative values can be attributed to the difficulty of reduction process due to de-protonation of the electroactive moiety of HL. Complex (L_2VO) registered two reduction peaks both of which are independent of pH. Peak 1c remained the same in the whole pH range while intensity of 2^{nd} peak decreased with increase in pH and disappeared in the basic region. Tin complex (L_2Sn) also exhibited two step reductions in which first process was just an electron transfer while in the second process proton transfer involved along with the electron transfer. Cobalt complex (L_2Co) registered only one pH independent peak in acidic media and no peak in basic pH range. Zinc complex (L_2Zn) exhibited a reduction process at a very low potential value of 0.0 V in strongly acidic solution of pH-2.0 which showed significant shifting by increasing pH of the medium. The reduced product of zinc complex was found to oxidize in an irreversible manner as its oxidation signal also appears in the reverse scan (**Fig. S10**). These findings are in agreement with the cyclic voltammetric response. Another reduction signal appeared at -0.67 V in acidic range which diminished with increase in pH. Number of electrons and protons involved in all these reduction processes were also calculated and applied for suggesting the mechanistic pathways of these processes (**Fig. S11 & S12**).

3.3. Biological Activities

3.3.1. Antidiabetic Activity

Mice treated with ligand HL showed significant decrease in blood glucose level as compared to the negative control group but showed increase as compared to positive control group ($p < 0.001$; $q = 8.329$ and $p < 0.001$; $q = 7.722$; **Fig. 6A**). Serum triglycerides concentration decreased significantly as compared to negative and positive control groups ($p < 0.001$; $q = 8.717$; and $p < 0.001$; $q = 15.415$; **Fig. 7A**), with no significant effects on serum cholesterol concentration (Fig. 7B). Animals treated with oxovanadium complex (L_2VO) significantly increased the blood glucose concentration as compared to the positive control group ($p < 0.001$; $q = 12.907$; Fig. 6B), a decrease in serum triglycerides concentration as compared to both positive and negative control groups ($p < 0.001$; $q = 13.336$ and $p < 0.001$; $q= 6.638$; Fig. 7A), while significant decrease occurred in serum cholesterol concentration as compared to both positive and negative control groups ($p < 0.05$; $q = 5.172$ and $p < 0.05$; $q =4.233$; Fig. 7B). L_2Sn treated group demonstrated a decrease in blood glucose concentration as compared to the negative control group ($p < 0.001$; $q = 18.037$; Fig. 6C), while a significant decrease occurred in serum triglycerides concentration relative to positive and negative control groups ($p < 0.001$; $q= 14.455$ and $p < 0.001$; $q = 7.758$; Fig. 7A). Serum cholesterol concentration decreased as compared to the positive control group ($p < 0.05$; $q = 4.430$; Fig. 7B). L_2Zn treated group showed a significant decrease in blood glucose level as compared to the negative control groups ($p < 0.001$; $q = 16.161$; Fig. 6D), a significant decrease in serum triglycerides concentration relative to positive and negative control groups ($p < 0.001$; $q= 13.416$ and $p < 0.05$; $q = 6.718$), while a decrease was noticeable in serum cholesterol concentration as compared to the positive group ($p < 0.05$; $q = 4.408$). L_2Co treated group showed significant decrease in blood glucose level as compared to negative control ($p < 0.001$; $q = 19.361$; Fig. 6E), while no effect was evident on serum triglycerides concentration and cholesterol concentrations (Figs. 7A & 7B).

3.3.2. *In Vitro* studies: Cytotoxicity analysis on HeLa

The synthesized Schiff base and its complexes were tested for their cytotoxic and anticancer activity against HeLa cell line at different concentrations (150, 100, 50, 10, and 5 µM) using SRB assay. SRB stained samples were visualized with Olympus IMT-2 inverted microscope (magnification 60X) and photographed (**Fig 8** A-Q). The viability curves (**Fig. 9**) were generated. The IC_{50} values of the complexes were calculated and listed in **Table 6**. HL (Fig 8 C, D, E) was found toxic to the cells in comparison to the untreated culture. A significant decrease in relative viability ($p < 0.05$) was observed with an IC_{50} value of 106.7 µM. L_2VO showed a strong influence on the cellular morphology and cells became more fiber like (Fig. 8 F-H). A strong decrease in relative viability ($p < 0.001$) of the treated cultures was observed and this complex showed two times higher toxicity to the cells compared to HL, with an IC_{50} value of 40.66 µM. Cells were found very sensitive to L_2Sn as only a few live cells existed at 100 and 50 µM (Fig 8J, K). The complex induced a highly significant decrease in relative viability ($p < 0.001$) of the cultures. The IC_{50} value of L_2Sn was 5.92 µM, thus cells showed 18 times more sensitivity to this complex in comparison to HL. L_2Zn showed a strong effect similar to L_2VO on the relative viability ($p < 0.001$) of the cultures with an IC_{50} value of 42.82 ($p < 0.001$; Fig 8 L, M, N). When compared to HL, L_2Co was found less toxic to the cultures with an IC_{50} value of 107.68 ($p > 0.05$; Fig 8 O, P, Q).

3.3.3. Inhibition of ALP

Literature survey reveals that Schiff bases show ALP inhibition activity and their complexes further enhance this activity. They can block the active sights of enzyme. Alkaline phosphatase uses a wide variety of phosphomonoesters to catalyze the transfer of phosphate groups to water

[21]. Experimental observations show that inhibition activity of HL is quite insignificant while the presence of metals enhances the deactivation of enzyme. The minimum activity of dibutyltin complex may be due to long alkyl chains having non-polar nature while Zn complex has shown excellent inhibition of nearly 90%. Inhibition profile is presented in **Fig. 10**.

3.3.4. Antimicrobial activities

Inhibitory action of HL and its metallic complexes was investigated against various strains of bacteria (*Bacillus subtilis, escherichia coli, pasturella multocida and staphlocuccus aureus*) and fungi (*Ganoderma lucidum aspergillus niger, alternaria alternate* and *penicillium notatum*) by disc diffusion method [37]. Streptomycin and fluconazole were selected as positive controls for antibacterial and antifungal screening tests, respectively. A recommended concentration of a test sample/reference drug (1mg/1mL of solvent) was introduced into the discs. The biologically active samples inhibited the bacterial/fungal growth around discs and the zones of inhibition were measured. The data have been summarized in **Tables 7 & 8**. The free ligand (HL) was almost inactive against the tested organisms. The coordination of ligand with metals (V, Sn, Zn, Co) induced antimicrobial activities in the complexes. Activity of the synthesized complexes was found in good agreement with their structures. The results demonstrate that each of the coordinated metals (V, Sn, Zn, Co) plays an important role in biological actions of these complexes [38]. The zinc complex (L_2Zn) was found the most potent inhibitor of bacteria/fungi while the vanadyl product (L_2VO) displayed the least activity among all the metal coordinated products. The coordination of ligand with the dibutyltin(IV) moiety appreciably enhanced the antibacterial/antifungal activity of L_2Sn. The inhibitory action of organotin(IV) compounds can be related to their interaction ability with DNA and proteins. After zinc, the highest antimicrobial

potential was observed for ligand-Co complex. The metal complexes were found more potent inhibitors of fungal culture as compared to bacterial growth [39].

3.4. Computational study

The DFT optimized structures of the HL and its complexes were obtained using 6-311++G^{**} and 6-311G^{++} basis sets, respectively. Numbering scheme of HL used for computational calculations is given in **Fig. S13**. Mullikan charges, dipole moments, optimization energies, spin multiplicity and point groups were calculated from the optimized structures (see **Table S2**). Comparison of bond lengths obtained from computational studies with that of X-ray analysis showed a good agreement with each other (see Table 2). NMR spectra of HL was calculated theoretically using 6-311++G^{**} basis set and compared with the experimental spectra (see **Table S3**). The computational findings reveal that the zwitter ionic form of HL is more stable than its enolic form. This structure is also consistent with its x-ray studies. Charge distribution values indicate that O atom of hydroxyl group and N atom of azomethine group are more negative in charge thus suggesting their preferred coordination with metal ions.

3.5 Redox mechanism of HL and complexes

The number of electrons and protons involved in redox processes were calculated from half peak width and slope values of E_p versus pH plots. The HL exhibited three oxidation peaks in positive potential window. Peak 1a was found to involve loss of one electron and one proton. On the basis of voltammetric results it is suggested that one electron and one proton are lost from the hydroxyl group at ortho position which may then convert to a free radical and possibly gets stabilized by dimerization or by adsorption at the electrode surface. It may either form a five membered ring with N atom or get converted to keto form with free radical resonating in the

whole benzene ring. It can also get adsorb on the GCE surface or dimerize as shown in **Scheme 4**. Similarly, peak 2a involves the loss of two electrons and two protons. This peak is assigned to azomethine group of HL present in keto form as shown in **Scheme 5**. On the basis of DPV results, the formation of 1-((2,4-dimethyl phenylimino)methylene)naphthalen-2(1H)-one is proposed.

Reduction of HL exhibited two separate peaks. $W_{1/2}$ value of peak 1c suggested loss of three protons along with four electrons per two molecules. This peak can be related to the conversion of azomethine group into -C-N bond (**Scheme 6**). Reduction peak 2c involves the reduction of -C=O moiety (keto form) by the gain of one electron and one proton. Oxidation of oxovanadium complex occurs in three different steps. DPV results show that peak 1a involves loss of two electrons along with two protons. Peak 2a remains independent in the whole studied pH range showing no involvement of proton while loss of three protons and four electrons per two molecules for peak 3a was calculated from DPV results. Organotin complex of HL was found to undergo oxidation in two steps in a similar manner. Electrochemical investigations demonstrated that pH independent peak 1a involves the loss of one electron while peak 2a involves loss of one proton along with one electron. Cobalt and zinc complexes were also found to oxidize in a similar manner but in case of zinc complex pH independent peak 2a appeared only in the basic pH regime. In case of HL, the two peaks are assigned to the oxidizable moieties –OH and –C=N present in the molecule.

4. Conclusion

A Schiff base HL and its four metallic complexes were synthesized and characterized by several techniques. FTIR, single crystal XRD, computational studies and spectroscopic results confirmed the existence of HL in zwitter ionic form along with usual enolic form. Photometric and redox

behavior of HL and complexes were found to be strongly pH dependent and irreversible. The computational studies were used as helping tools in suggesting the redox mechanism of the electrophores of the analytes. Schiff base and its complexes exhibit excellent biological activities and toxicity to cancer cells. These studies provide preliminary screening data for diabetic, fungal, microbial and cancer treatment. Further studies are required to precisely evaluate the underlying mechanism of their activity in vitro as well as in vivo.

Acknowledgements

The authors gratefully acknowledge the financial support of Quaid-i-Azam University, Islamabad and Higher Education Commission of Pakistan.

References

[1] K.N. Venugopala, B.S. Jayashree, Microwave-Induced Synthesis of Schiff Bases of Aminothiazolyl Bromocoumarins as Antibacterials, Indian Journal of Pharmaceutical Sciences, 70 (2008) 88-91.

[2] S. Wadher, M. Puranik, N. Karande, P. Yeole, Synthesis and biological evaluation of Schiff base of dapsone and their derivative as antimicrobial agents, International Journal of PharmTech Research, 1 (2009) 22-33.

[3] N. Solak, S. Rollas, Synthesis and antituberculosis activity of 2-(aryl/alkylamino)-5-(4-aminophenyl)-1, 3, 4-thiadiazoles and their Schiff bases, Arkivoc, 12 (2006) 173-181.

[4] A.S. Abu-Khadra, R.S. Farag, A.E.D.M. Abdel-Hady, Synthesis, characterization and antimicrobial activity of Schiff base (E)-N-(4-(2-hydroxybenzylideneamino) phenylsulfonyl) acetamide metal complexes, American Journal of Analytical Chemistry, 7 (2016) 233-245.

[5] Z. Cimerman, S. Miljanić, N. Galić, Schiff bases derived from aminopyridines as spectrofluorimetric analytical reagents, Croatica Chemica Acta, 73 (2000) 81-95.

[6] M. Kabak, A. Elmali, Y. Elerman, Keto–enol tautomerism, conformations and structure of N-(2-hydroxy-5-methylphenyl), 2-hydroxybenzaldehydeimine, Journal of Molecular Structure, 477 (1999) 151-158.

[7] P. Comon, Independent component analysis, a new concept?, Signal Processing, 36 (1994) 287-314.

[8] P.G. Cozzi, Metal–Salen Schiff base complexes in catalysis: practical aspects, Chemical Society Reviews, 33 (2004) 410-421.

[9] S. CHANDRA, EPR and electronic spectral studies on copper (II) complexes of some NO donor ligands, Journal of the Indian Chemical Society, 81 (2004) 203-206.

[10] S. Kumar, D.N. Dhar, P. Saxena, Applications of metal complexes of Schiff bases—a review, Journal of Scientific and Industrial Research, 68 (2009) 181-187.

[11] G.J. Britovsek, V.C. Gibson, S. Mastroianni, D.C. Oakes, C. Redshaw, G.A. Solan, A.J. White, D.J. Williams, Imine versus amine donors in iron-based ethylene polymerisation catalysts, European Journal of Inorganic Chemistry, 2001 (2001) 431-437.

[12] D.M. Boghaei, S. Mohebi, Non-symmetrical tetradentate vanadyl Schiff base complexes derived from 1, 2-phenylene diamine and 1, 3-naphthalene diamine as catalysts for the oxidation of cyclohexene, Tetrahedron, 58 (2002) 5357-5366.

[13] S.-Y. Liu, D.G. Nocera, A simple and versatile method for alkene epoxidation using aqueous hydrogen peroxide and manganese salophen catalysts, Tetrahedron Letters, 47 (2006) 1923-1926.

[14] A. Budakoti, M. Abid, A. Azam, Synthesis and antiamoebic activity of new 1-N-substituted thiocarbamoyl-3, 5-diphenyl-2-pyrazoline derivatives and their Pd (II) complexes, European Journal of Medicinal Chemistry, 41 (2006) 63-70.

[15] J.F. Lawrence, C. Renault, R.W. Frei, Fluorogenic labeling of organophosphate pesticides with dansyl chloride: Application to residue analysis by high-pressure liquid chromatography and thin-layer chromatography, Journal of Chromatography A, 121 (1976) 343-351.

[16] P. Kavitha, M.R. Chary, B. Singavarapu, K.L. Reddy, Synthesis, characterization, biological activity and DNA cleavage studies of tridentate Schiff bases and their Co (II) complexes, Journal of Saudi Chemical Society, 20 (2016) 69-80.

[17] M.A. Munoz-Hernandez, M.L. McKee, T.S. Keizer, B.C. Yearwood, D.A. Atwood, Six-coordinate aluminium cations: characterization, catalysis, and theory, Journal of the Chemical Society, Dalton Transactions, (2002) 410-414.

[18] B.K. Rai, Synthesis, spectral and antimicrobial study of Co (II), Ni (II) and Cu (II) complexes with Schiff bases of 3-pyridinyl n-pentyl ketone, Indian Council of Chemistry, 25 (2008) 137-141.

[19] A.E. Taggi, A.M. Hafez, H. Wack, B. Young, D. Ferraris, T. Lectka, The development of the first catalyzed reaction of ketenes and imines: catalytic, asymmetric synthesis of β-lactams, Journal of the American Chemical Society, 124 (2002) 6626-6635.

[20] E. Jungreis, S. Thabet, Analytical applications of Schiff bases, Chelates in Analytical Chemistry, 2 (1969) 149-177.

[21] A. Rauf, A. Shah, S. Abbas, U.A. Rana, S.U.-D. Khan, S. Ali, R. Qureshi, H.B. Kraatz, F. Belanger-Gariepy, Synthesis, spectroscopic characterization and pH dependent photometric and electrochemical fate of Schiff bases, Spectrochimica Acta Part A: Molecular and Biomolecular Spectroscopy, 138 (2015) 58-66.

[22] P. Skehan, R. Storeng, D. Scudiero, A. Monks, J. McMahon, D. Vistica, J.T. Warren, H. Bokesch, S. Kenney, M.R. Boyd, New colorimetric cytotoxicity assay for anticancer-drug screening, Journal of the National Cancer Institute, 82 (1990) 1107-1112.

[23] M. Jabeen, S. Ali, S. Shahzadi, M. Shahid, Q. Khan, S. Sharma, K. Qanungo, Homobimetallic complexes of ligand having O-and S-donor sites with same and different di-and trialkyl/aryltin (IV) moiety: their synthesis, spectral characterization and biological activities, Journal of the Iranian Chemical Society, 9 (2012) 307-320.

[24] A. Shah, E. Nosheen, S. Munir, A. Badshah, R. Qureshi, Z. Rehman, N. Muhammad, H. Hussain, Characterization and DNA binding studies of unexplored imidazolidines by electronic absorption spectroscopy and cyclic voltammetry, Journal of Photochemistry and Photobiology B: Biology, 120, (2013) 90–97.

[25] E. Conpolat and M. Kaya, Studies on mononuclear chelates derived from substituted Schiff-base ligands (part 2): synthesis and characterization of a new 5-bromosalicyliden-p-aminoacetophenone oxime and its complexes with Co(II), Ni(II), Cu(II) and Zn(II). Journal of Coordination Chemistry, 57 (2004) 1217-1223.

[26] B.H. Al-Zaid, N.J. Al-Obaidi, Synthesis and Spectral Studies of Cr(III), Mn(II), Co(II), Ni(II), Cu(II) and Cd(II) Complexes with New Bidentate (N,O) Schiff Base Ligand bearing an Oxime functional group, Journal of The College of Basic Education, 20 (2015) 939-948.

[27] M.K. Nazeeruddin, S.M. Zakeeruddin, K. Kalyanasundaram, Enhanced intensities of the ligand-to-metal charge-transfer transitions in Ru(II1) and Os(II1) complexes of substituted bipyridines, Journal of Physical Chemistry, 97 (1993) 9607-9612.

[28] M.M.H. Khalil, E.H. Ismail, G.G. Mohamed, E.M. Zayed, A. Badr, Synthesis and characterization of a novel schiff base metal complexes and their application in determination of iron in different types of natural water, Open Journal of Inorganic Chemistry, 2 (2012) 13-21.

[29] S.L. Reddy, T. Endo, G.S. Reddy, Electronic (absorption) spectra of 3d transition metal complexes. In: Advanced Aspects of Spectroscopy, Eds. Farrukh, M. A., InTech (2012).

[30] A. Shah, R. Qureshi, A.M. Khan, R.A. Khera, F.L. Ansari, Electrochemical behavior of 1-ferrocenyl-3-phenyl-2-propen-1-one on glassy carbon electrode and evaluation of its interaction parameters with DNA, Journal of the Brazilian Chemical Society, 21 (2010) 447-451.

[31] A. Shah, V.C. Diculescu, R. Qureshi, A.M. Oliveira-Brett, Electrochemical behaviour of dimethyl-2-oxoglutarate on glassy carbon electrode, Bioelectrochemistry, 77, (2010) 145–150.

[32] Erum Nosheen, A. Shah, A. Badshah, Z. Rehmana, H. Hussain, R. Qureshi, S. Ali, M. Siddiq, A.M. Khan, Electrochemical oxidation of hydantoins at glassy carbon electrode, Electrochimica Acta, 80 (2012) 108–117.

[33] A.H. Shah, W. Zaid, A. Shah, U.A. Rana, H. Hussain, M.N. Ashiq, R. Qureshi, A. Badshah, M.A. Zia, H.-B. Kraatz, pH dependent electrochemical characterization, computational studies and evaluation of thermodynamic, kinetic and analytical parameters of two phenazines, Journal of The Electrochemical Society, 162 (2015) H115-H123.

[34] A.H. Shah, A. Shah, S.U.-D. Khan, U.A. Rana, H. Hussain, S.B. Khan, R. Qureshi, A. Badshah, A. Waseem, Probing the pH dependent electrochemistry of a novel quinoxaline carboxylic acid derivative at a glassy carbon electrode, Electrochimica Acta, 147 (2014) 121-128.

[35] A.H. Shah, A. Shah, U.A. Rana, S.U.D. Khan, H. Hussain, S.B. Khan, R. Qureshi, A. Badshah, Redox mechanism and evaluation of kinetic and thermodynamic parameters of 1, 3-Dioxolo [4, 5-g] pyrido [2, 3-b] quinoxaline using electrochemical techniques, Electroanalysis, 26 (2014) 2292-2300.

[36] V.C. Diculescu, A. Militaru, A. Shah, R. Qureshi, L. Tugulea, A.M. Oliveira-Brett, Redox mechanism of lumazine at a glassy carbon electrode, Journal of Electroanalytical Chemistry, 647, (2010) 1–7.

[37] S. Hussain, I.H. Bukhari, S. Ali, S. Shahzadi, M. Shahid, K.S. Munawar, Synthesis and spectroscopic and thermogravimetric characterization of heterobimetallic complexes with Sn (IV) and Pd (II); DNA binding, alkaline phosphatase inhibition and biological activity studies, Journal of Coordination Chemistry, 68 (2015) 662-677.

[38] N.R. Bhalodia, V.J. Shukla, Antibacterial and antifungal activities from leaf extracts of Cassia fistula l.: An ethnomedicinal plant, Journal of Advanced Pharmaceutical Technology & Research, 2 (2011) 104-109.

[39] Q.K. Huynh, J.R. Borgmeyer, C.E. Smith, Isolation and characterization of a 30 kDa protein with antifungal activity from leaves of Engelmannia pinnatifida, Biochemical Journal, 316 (1996) 723-727.

List of Figures

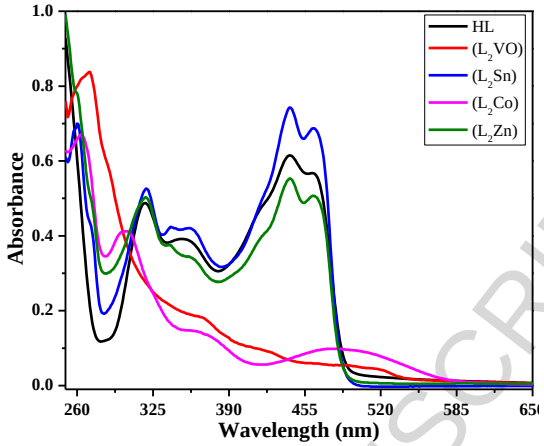

Fig. 1. UV-Vis spectra of 20 μM HL, L_2VO, L_2Sn, L_2Co and L_2Zn.

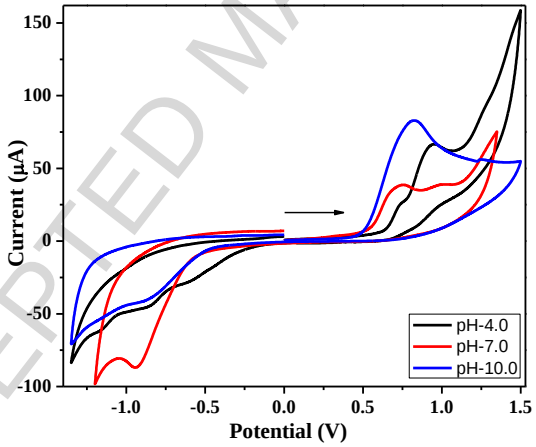

Fig. 2: Cyclic voltammograms of HL obtained at 100 mVs^{-1} in solutions of pH 4.0, 7.0 and 10.0.

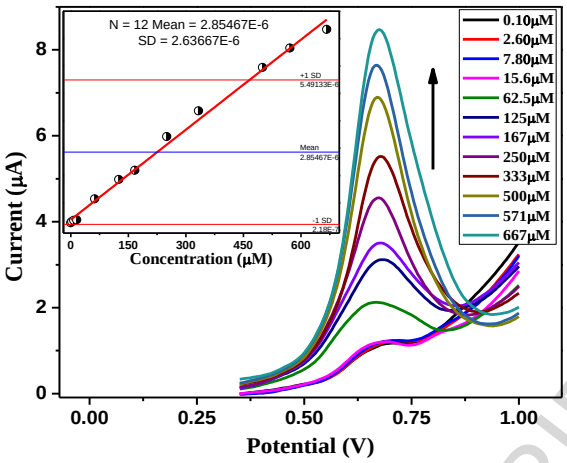

Fig. 3: Square wave voltammograms of different concentrations of (L_2Sn) obtained at a scan rate 100 mV/s in pH 7.0, inset shows I_p as a function of concentration

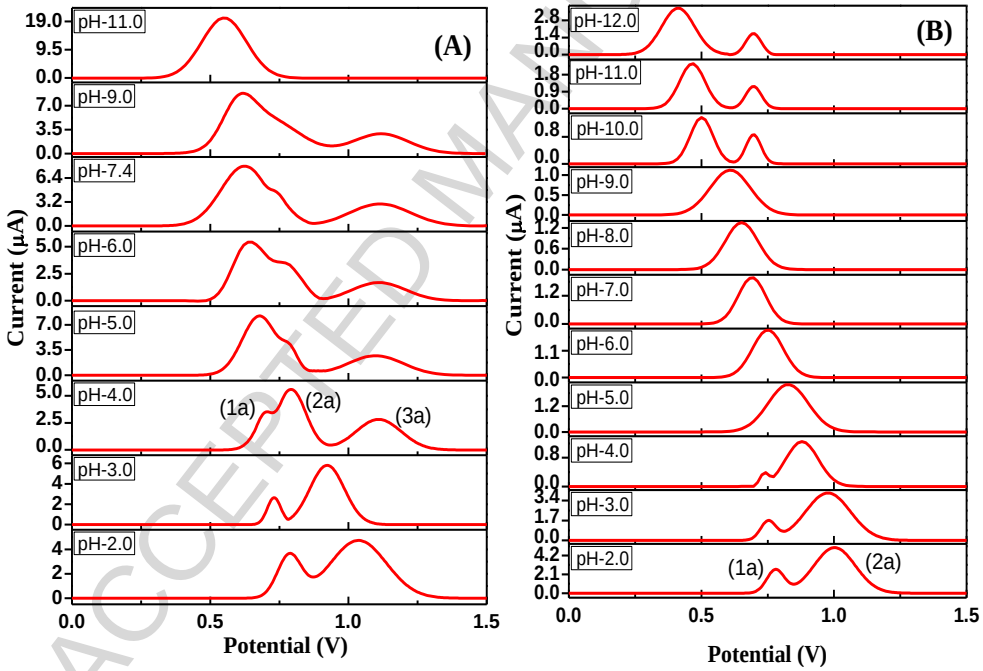

Fig. 4. Differential pulse voltammograms recorded in different pH media at 5 mVs^{-1} showing oxidation of HL (A) and L_2Co (B).

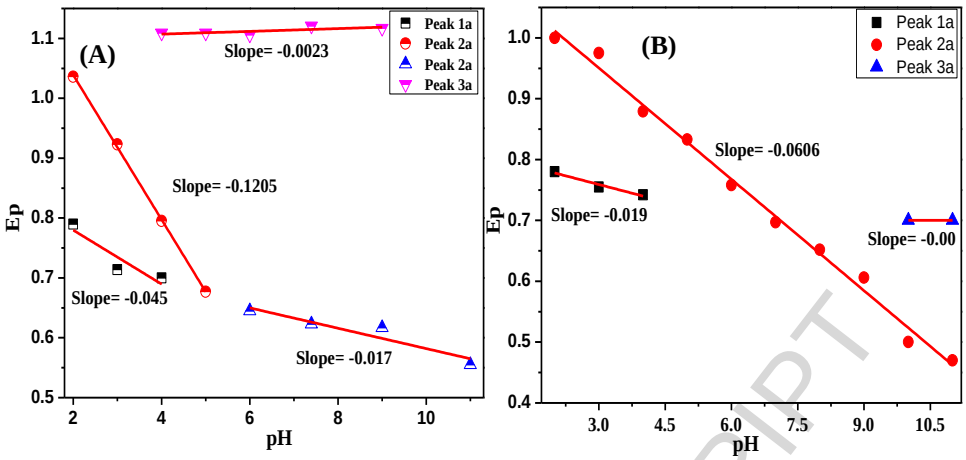

Fig. 5. Plots of oxidation potentials versus pH for HL (A) and (L_2Co) (B)

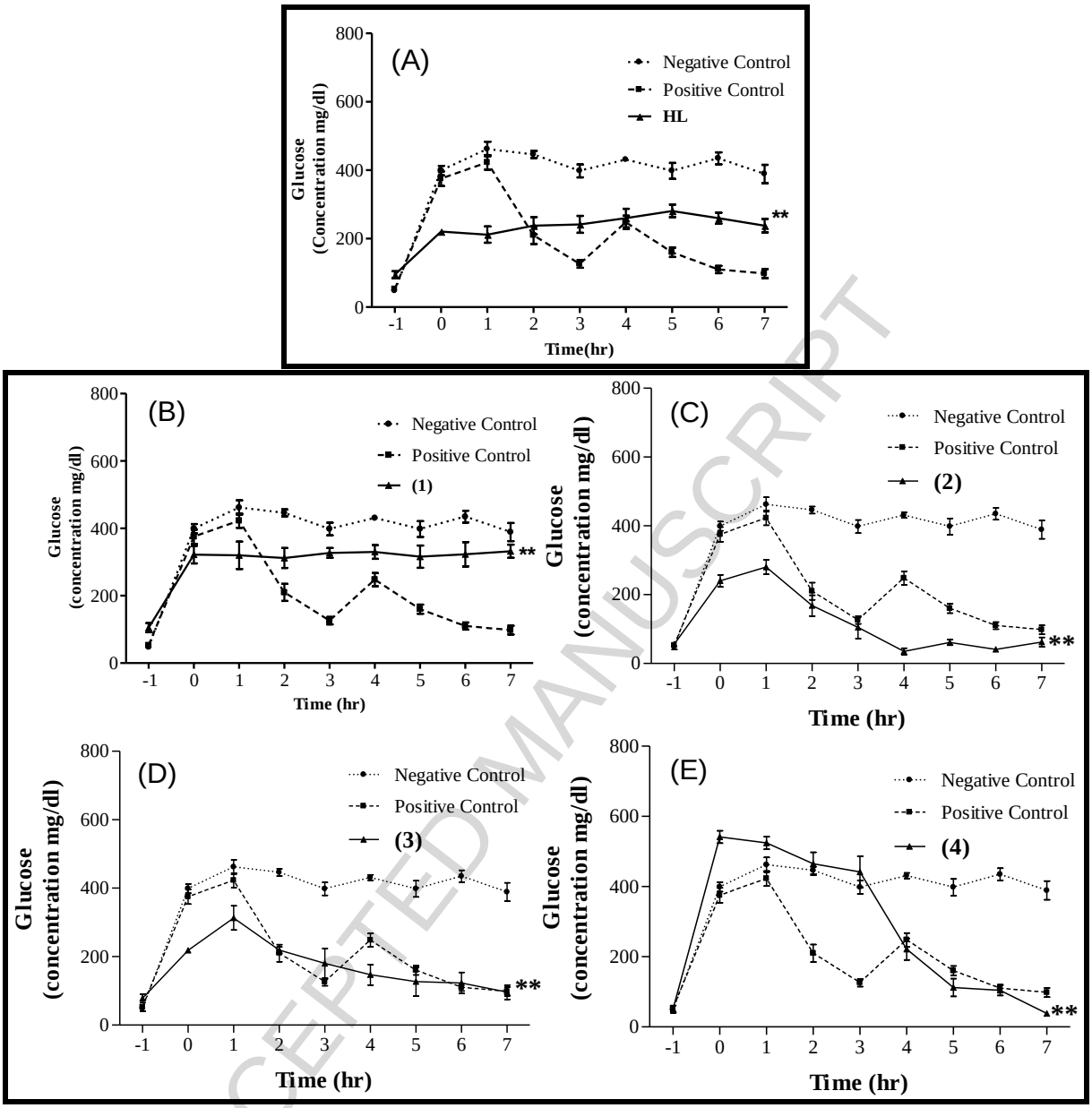

Fig. 6. Plasma glucose in mice treated with HL, L_2VO (1), L_2Sn (2), L_2Zn (3) and L_2Co (4) compound groups.

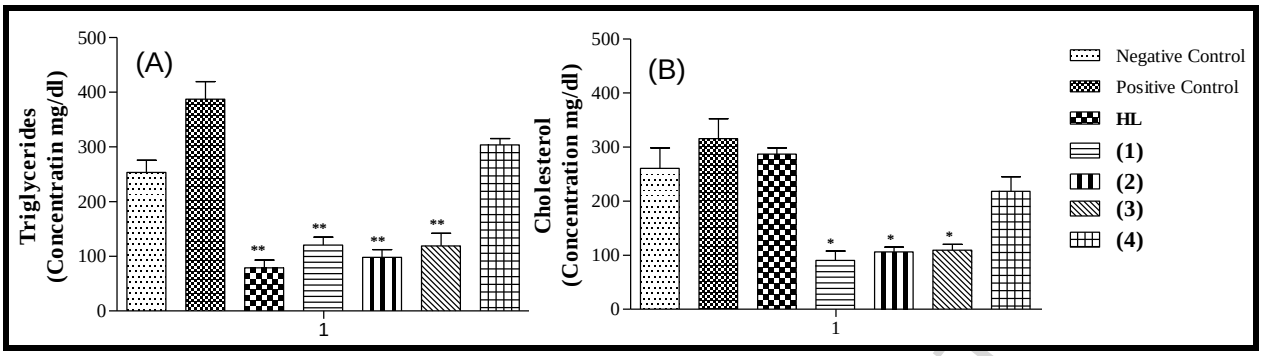

Fig.7. (A) Except cobalt complex (L_2Co), mice treated with compounds HL, L_2VO, L_2Sn, and L_2Zn decreased serum triglycerides concentration as compared to both control groups ($p<0.001$). (B) Oxo vanadium complex (L_2VO) treated group has a significant effect on decreasing serum cholesterol concentration as compared to both control groups ($p<0.05$), while groups treated with complexes (L_2Sn) and (L_2Zn) decreased cholesterol concentration as compared to positive control group ($p<0.05$). Data is presented as mean ± SEM.

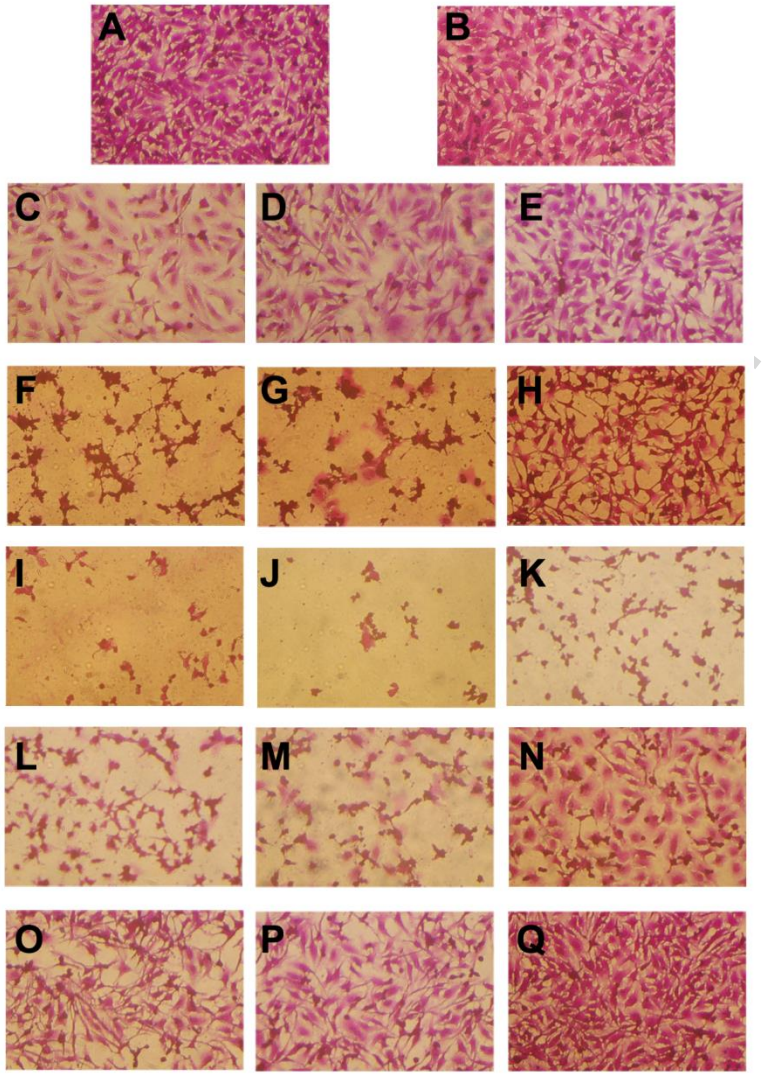

Fig. 8: Effect of HL, (L_2VO), (L_2Sn), (L_2Zn) and (L_2Co) complexes on HeLa cells. Cultures treated with different concentrations of the compounds for 24 h were stained with SRB, visualized with Olympus IMT-2 inverted microscope (magnification 60X) and photographed. A. Untreated control, B. Solvent (5% DMSO + 95% Ethanol) treated sample, C, D, E, Treated with 100, 50, and 10µM of HL, respectively, F, G, H, Treated with 100, 50, and 10µM of (L_2VO), respectively, I, J, K, Treated with 100, 50, and 10µM of (L_2Sn), respectively, L, M, N, Treated with 100, 50, and 10µM of (L_2Zn), respectively, O, P, Q, Treated with 100, 50, and 10µM of (L_2Co), respectively.

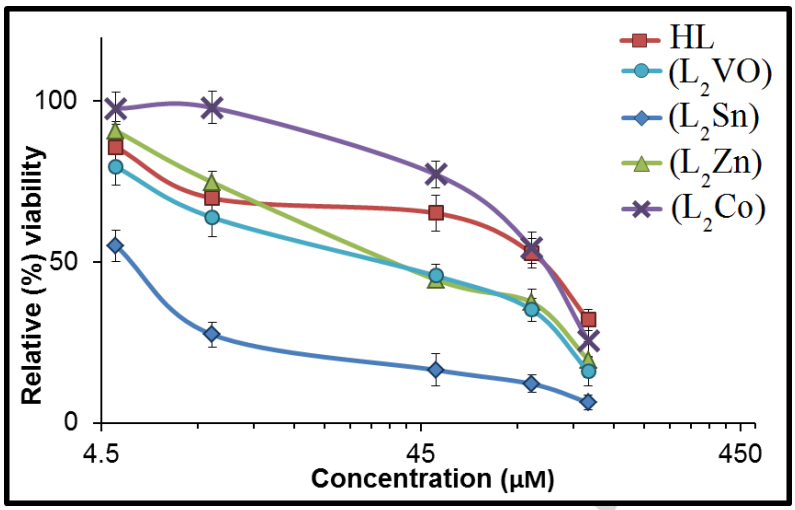

Fig. 9: Viability curves for HL, (L_2VO), (L_2Sn), (L_2Zn) and (L_2Co) complexes in HeLa. Cultures were exposed to serial dilutions of the compounds (150, 100, 50, 10, and 5 μM) for 24 h and relative (%) viabilities (mean±SD) were measured using SRB Assay.

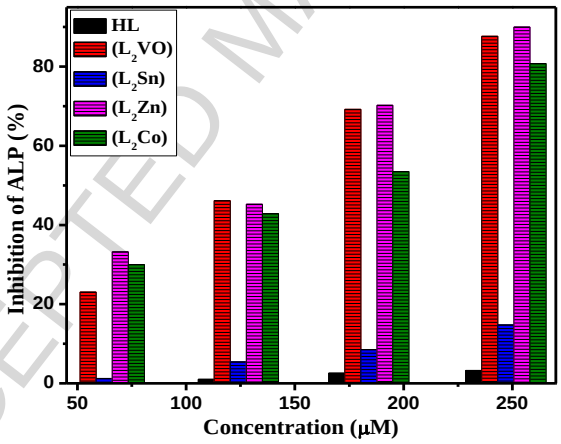

Fig. 10. Inhibition profile of alkaline phosphatase (ALPs) at different concentrations of HL, L_2VO, L_2Sn, L_2Zn and L_2Co.

List of Schemes

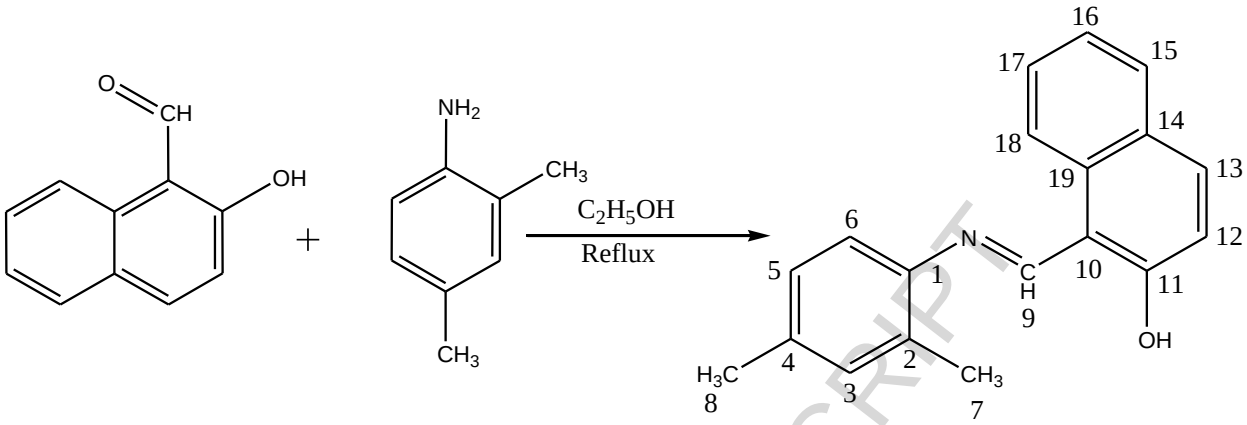

Scheme 1. Synthesis of Schiff base HL and its numbering scheme.

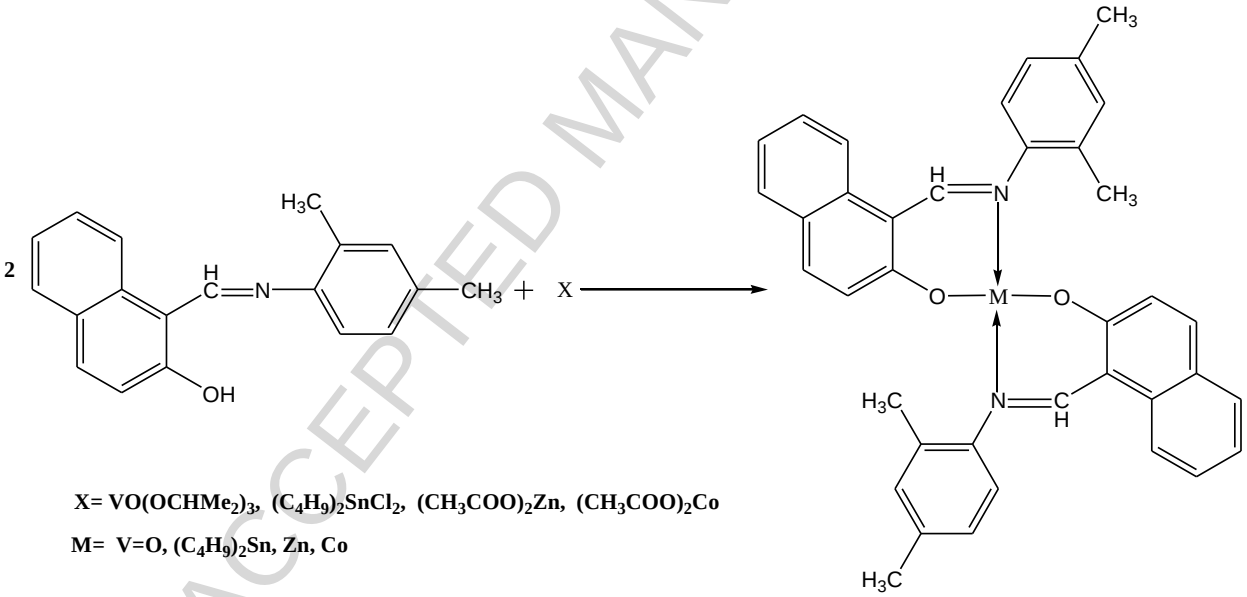

X= $VO(OCHMe_2)_3$, $(C_4H_9)_2SnCl_2$, $(CH_3COO)_2Zn$, $(CH_3COO)_2Co$

M= V=O, $(C_4H_9)_2Sn$, Zn, Co

Scheme 2. Synthesis of metal complexes of HL.

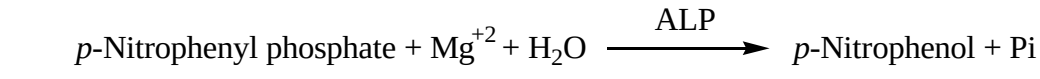

Scheme 3. Hydrolysis of alkaline phosphatase.

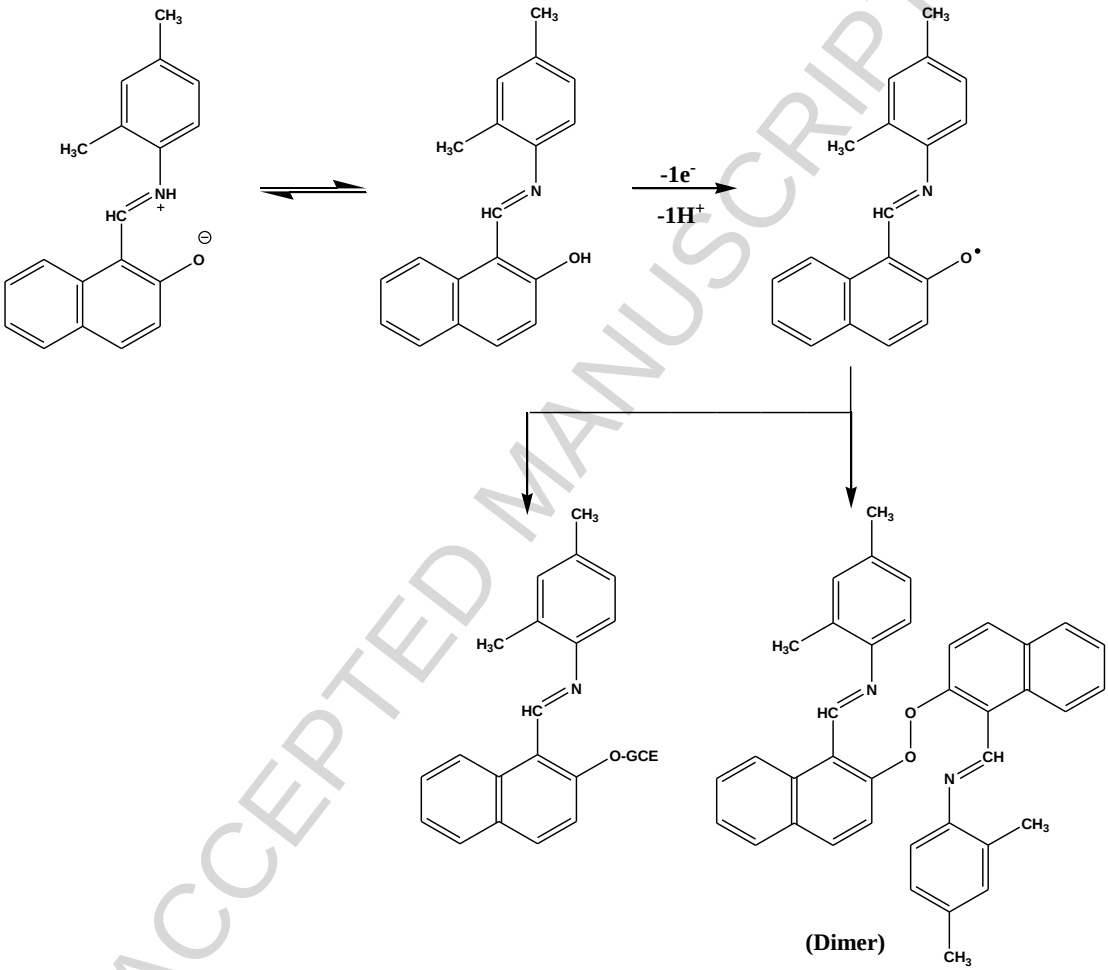

Scheme 4. Proposed oxidation mechanism of HL corresponding to peak 1a.

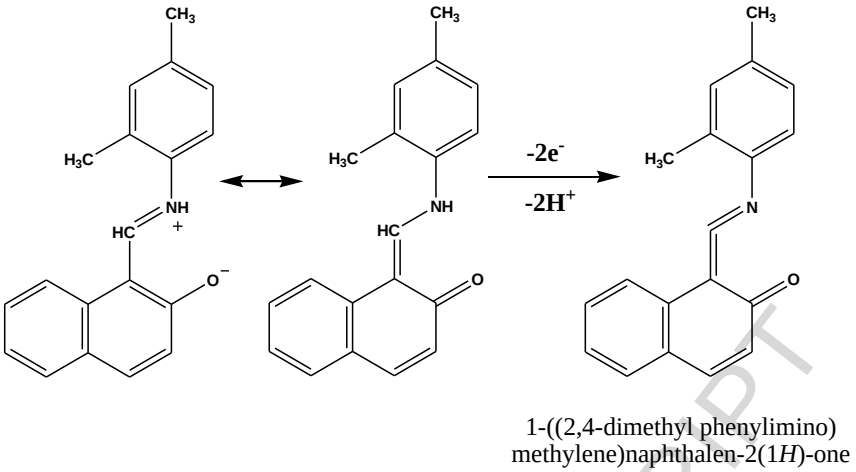

1-((2,4-dimethyl phenylimino) methylene)naphthalen-2(1*H*)-one

Scheme 5. Proposed oxidation mechanism of HL corresponding to peak 2a.

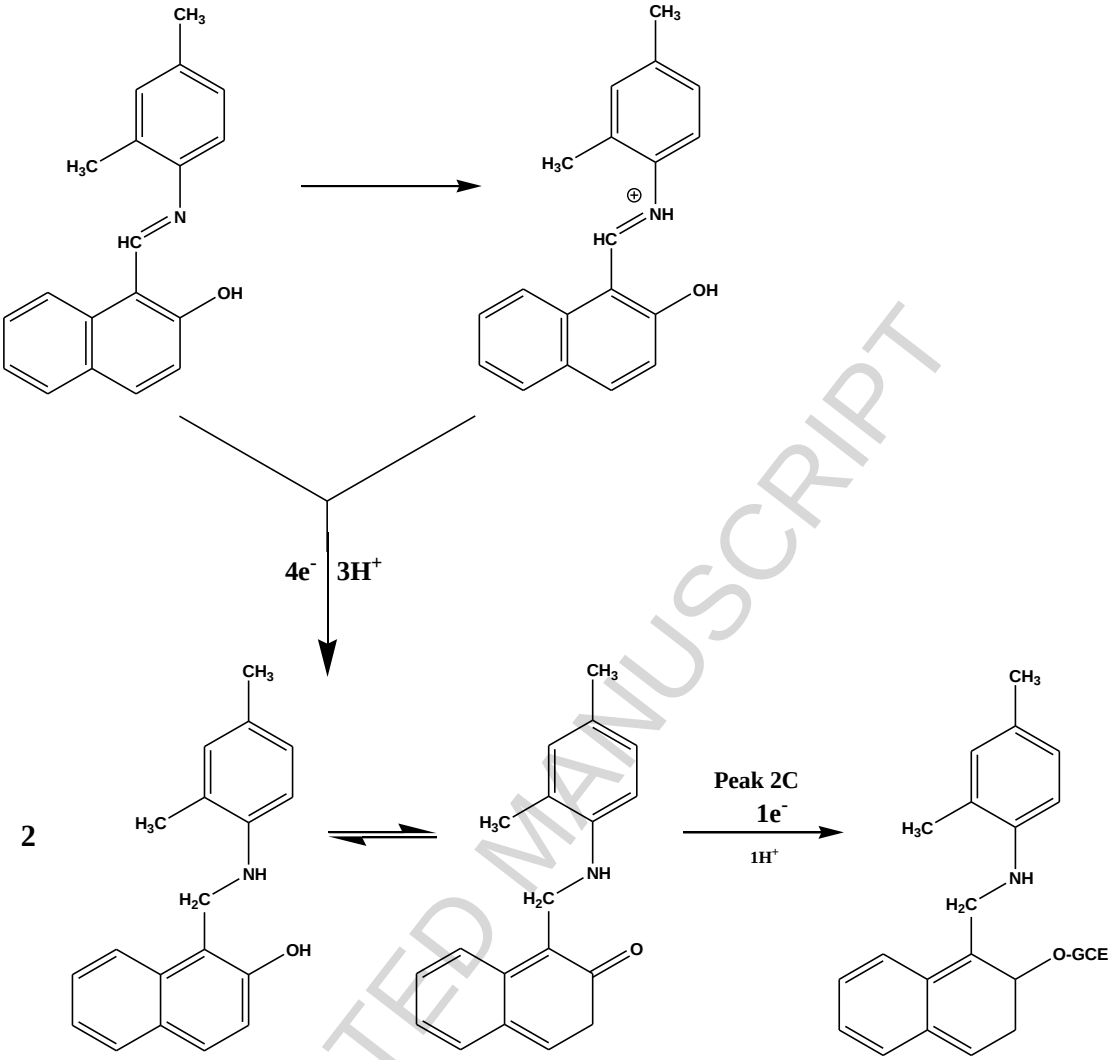

Scheme 6. Proposed reduction mechanism corresponding to peak 1c and 2c.

Tables

Table 1. Thermogravimetric data of complexes L_2VO and L_2Co.

Complexes	Temp. range (^oC)	Evolved components	% Weight loss		% Residue	
			Observed	Calculated	Observed	Calculated
(L_2VO)	24-765	$2C_8H_9N$	38.61	38.71	$C_9H_6O_3V$	
	765-951	$C_{13}H_8$	26.91	26.67	34.48	34.62
(L_2Co)	198-658	$C_{38}H_{32}N_2$	84.55	85.03	CoO_2	
					15.45	14.97

Table 2. Selected experimental and calculated geometric parameters of HL.

Bond distances (Å)				**Exp.**	**Calc.**	Δ
O1	C1			1.292	1.310	0.018
N1	C11			1.306	1.315	0.009
N1	C12			1.408	1.402	-0.006
N1	H1			1.020	1.090	0.070
C1	C10			1.429	1.401	-0.028
C10	C11			1.416	1.448	0.032
C12	C13			1.401	1.401	0.000
C12	C17			1.393	1.401	0.008
C13	C18			1.488	1.510	0.022
C15	C19			1.509	1.514	0.005
C18	H18A			0.960	1.070	0.110
C19	H19C			0.960	1.070	0.110
Bond angles (°)				**Exp.**	**Calc.**	Δ
C11	N1	C12		126.0	121.8	-4.2
C11	N1	H1		112.0	109.4	-2.6
C2	C1	C10		118.4	119.1	0.7
O1	C1	C10		122.0	122.3	0.3
O1	C1	C2		119.6	119.4	-0.2
N1	C11	C10		122.8	124.1	1.3
N1	C12	C17		122.8	122.4	-0.4
C14	C15	C16		117.7	118.0	0.3
N1	C11	H11		119.0	120.3	1.3
C13	C12	C17		119.7	119.6	-0.1
C12	C13	C14		117.6	118.4	0.8
C13	C18	H18C		109.0	109.5	0.5
H18A	C18	H18B		109.0	109.4	0.4
Torsion angles (°)				**Exp.**	**Calc.**	Δ
C12	N1	C11	C10	179.2	178.6	-0.6
C11	N1	C12	C13	170.9	177.0	6.1
O1	C1	C10	C11	-4.8	-0.8	4
C1	C10	C11	N1	3.7	-0.1	-3.8
N1	C12	C13	C18	-1.2	-1.2	0.0

Table 3. Hydrogen-bonding geometry (Å, °) of the HL crystal.

D	H	A	d(D-H)/Å	d(H-A)/Å	d(D-A)/Å	D-H-A/°
N1	H1	O1	1.0200	1.6700	2.5413	141.00

Table 4. Diffusion coefficients and heterogeneous electron transfer rate constant values for HL, L_2VO, L_2Sn, L_2Zn and L_2Co.

Compounds	$D_o \times 10^6$	$k_s \times 10^5$
HL	7.514	4.750
L_2VO	0.040	0.021
L_2Sn	0.144	0.260
L_2Zn	0.507	0.390
L_2Co	0.620	0.563

Table 5. LOD and LOQ values for HL, L_2VO, L_2Sn, L_2Zn and L_2Co.

Compounds	**LOD (µM)**	**LOQ (µM)**
HL	7.21	24.03
L_2VO	17.6	58.60
L_2Sn	3.48	11.60
L_2Zn	0.10	0.33
L_2Co	5.63	18.77

Table 6. IC_{50} value (µM) of HL, L_2VO, L_2Sn, L_2Zn and L_2Co complexes for HeLa cell line.

Compound	**IC_{50} value (µM)**
HL	106.70
L_2VO	40.66
L_2Sn	5.92
L_2Zn	42.82
L_2Co	107.68

Table 7. Comparison of antibacterial activities of HL and complexes.

Compounds	**Average zone of inhibition (mm)**			
	E. coli	***B. subtilis***	***S. aureus***	***P. multocida***
Streptomycin	$30^{a} \pm 0.27$	$30^{ab} \pm 0.19$	$30^{ab} \pm 0.22$	$30^{a} \pm 0.29$
HL	0	0	$14^{c} \pm 0.18$	$14^{c} \pm 0.15$
L_2VO	$18^{c} \pm 0.27$	$15^{c} \pm 0.19$	$20^{bc} \pm 0.17$	$17^{bc} \pm 0.22$
L_2Sn	$22^{bc} \pm 0.17$	$19^{bc} \pm 0.13$	$22^{bc} \pm 0.22$	$25^{ab} \pm 0.13$
L_2Zn	$28^{ab} \pm 0.12$	$31^{a} \pm 0.14$	$32^{a} \pm 0.18$	$33^{a} \pm 0.11$
L_2Co	$25^{ab} \pm 0.13$	$29^{ab} \pm 0.19$	$28^{ab} \pm 0.19$	$31^{ab} \pm 0.11$

Concentration = 1mg/mL in DMSO; 0 = No activity, 5-10 = Activity present, 11-25 = Moderate activity, 26-40 = Strong activity; Antibacterial values are mean ± S.D of samples analyzed individually in triplicate at $p < 0.1$; Different letters in superscripts indicate significant differences. a = maximum activity, b = intermediate activity, c = minimum activity, ab = activity between maximum and intermediate and bc = activity between intermediate and minimum.

Table 8. Comparison of antifungal activities of HL and complexes.

Compounds	Average zone of inhibition (mm)			
	A. alternate	***G. lucidum***	***A. niger***	***P. notatum***
Fluconazole	$38^{a} \pm 0.41$	$41^{ab} \pm 0.52$	$40^{ab} \pm 0.36$	$35^{ab} \pm 0.27$
HL	$19^{c} \pm 0.22$	$13^{c} \pm 0.21$	$18^{c} \pm 0.33$	$20^{c} \pm 0.27$
L_2VO	$22^{bc} \pm 0.25$	$25^{bc} \pm 0.29$	$31^{ab} \pm 0.28$	$36^{ab} \pm 0.22$
L_2Sn	$25^{bc} \pm 0.26$	$39^{ab} \pm 0.19$	$33^{c} \pm 0.25$	$30^{bc} \pm 0.21$
L_2Zn	$36^{ab} \pm 0.12$	$42^{a} \pm 0.14$	$45^{a} \pm 0.08$	$40^{a} \pm 0.18$
L_2Co	$32^{ab} \pm 0.12$	$40^{ab} \pm 0.18$	$38^{ab} \pm 0.17$	$34^{ab} \pm 0.16$

Concentration = 1mg/mL in DMSO; 0 = No activity, 5-10 = Activity present, 11-25 = Moderate activity, 26-40 = Strong activity; Antifungal values are mean ± S.D of samples analyzed individually in triplicate at $p < 0.1$; Different letters in superscripts indicate significant differences. a = maximum activity, b = intermediate activity, c = minimum activity, ab = activity between maximum and intermediate and bc = activity between intermediate and minimum.

Graphical Abstract

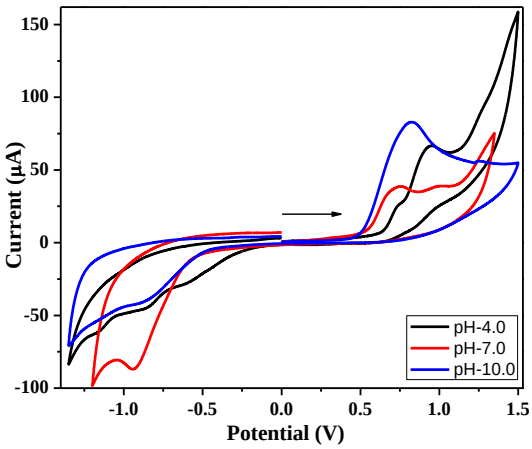

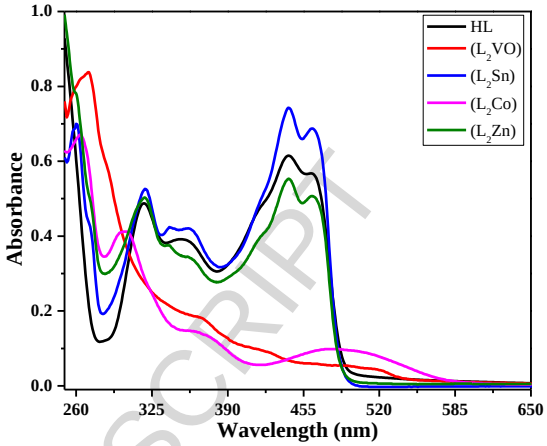

Highlights:

- A novel Schiff base and its four metallic complexes were synthesized
- Structural characterization were performed using various structure elucidation techniques
- Photometric investigations of the Schiff base and its complexes were performed
- The detailed redox behaviour of the compounds in different pH media was proposed
- Various biological activities of the synthesized compounds were studied